AALBORG UNIVERSITY

DENMARK

Evaluation of the Load-Displacement Relationships for Large-Diameter Piles in Sand

Sørensen, Søren Peder Hyldal; Brodbaek, K. T.; Moller, M.; Augustesen, Anders Hust; Ibsen, Lars Bo

[Link to publication from Aalborg University](#)

Paper 244

Evaluation of the Load-Displacement Relationships for Large-Diameter Piles in Sand

S.P.H. Sorensen, K.T. Brodbaek, M. Moller
A.H. Augustesen and L.B. Ibsen
Department of Civil Engineering
Aalborg University, Denmark

Abstract

For laterally loaded piles in sand with diameters up to 6 m, e.g. monopiles used as foundations for offshore wind turbines, there is no approved design procedure. The p–y curve method, given in offshore design regulations, is usually employed for the design of monopiles. However, this method was developed for slender piles with diameters much less than 6 m and it is based on a limited number of tests. The aim of the present work is to extend the p–y curve method to large-diameter non-slender piles by considering the effects of the pile diameter on the soil response. The main focus is the initial stiffness of the p–y curves. The evaluation is based on experimental work as well as three-dimensional numerical analyses in the commercial programme $FLAC^{3D}$.

Keywords: monopile, sand, p–y curves, Winkler model approach, geotechnical engineering, $FLAC^{3D}$, laboratory tests.

1 Introduction

Several concepts for offshore wind turbine foundations exist. The choice of foundation concept primarily depends on site conditions and the dominant type of loading. At great water depths the most common foundation concept is monopiles, which are single steel pipe piles driven open-ended. Recently installed monopiles have diameters around 4 to 6 m and a pile slenderness ratio (L/D) around 5 where L is the embedded length and D is the outer pile diameter. The maximum forces acting on a 3.5 MW offshore wind turbine foundation at the mudline is, according to Ubilla et al. [1], in the order of 4 MN in horizontal load, 6 MN in vertical load, and 120 MNm in overturning moment. Hence, a monopile foundation for an offshore wind turbine is highly subjected to lateral loading.
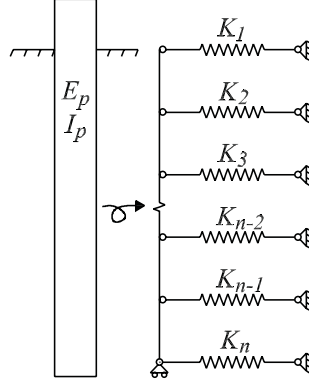
Figure 1: Winkler model approach. K denotes the stiffness of the elastic foundation while E_p and I_p are the Young's modulus of elasticity and second moment of inertia for the pile, respectively. The circles indicate hinges.

In current design of laterally loaded offshore monopiles, p–y curves are normally employed. A p–y curve describe the non-linear relationship between the soil resistance acting against the pile wall, p, and the lateral deflection of the pile, y. Several formulations of p–y curves exist depending on the type of soil. These formulations are originally formulated to be employed in the offshore oil and gas sector. However, they are also used for offshore wind turbine foundations, although piles with significantly larger diameter and significantly smaller slenderness ratio are employed for this type of foundation. In traditional design a Winkler approach is often employed in which the pile is modelled as a beam on an elastic foundation, cf. Figure 1. The elastic foundation consists of a number of springs with spring stiffness, K_i, given by means of p–y curves. When using the Winkler approach the soil continuity is not taken into account as the springs are considered uncoupled.

The p–y curve for sand employed in the offshore design regulations, e.g. DNV [2] and API [3], are given in Equation (1).

$$p(y) = Ap_u \tanh\left(\frac{kx}{Ap_u}y\right) \tag{1}$$

in which A is a factor corresponding to static or cyclic analyses, p_u is the ultimate soil resistance, k is the initial modulus of subgrade reaction and x is the depth measured from soil surface. k is determined in terms of the angle of internal friction or the relative density and governs the initial slope of the p–y curves. Hereby, the initial stiffness of the p–y curves is assumed independent of the pile properties.

The hyperbolic expression is based on the testing of two identical, instrumented piles installed at Mustang Island, Texas as desribed by Cox et al. [4]. The tests included a total of seven load cases. Furthermore, the tests were conducted for only one pile diameter, one type of sand, and for circular pipe piles. A change in any of these factors might affect the behaviour of a laterally loaded pile. Due to the very limited number of full-scale tests performed to validate the method, the influence of

2

a broad spectra of parameters on the p–y curves are still to be clarified. Especially when considering offshore wind turbine foundations a validation of stiff piles with a slenderness ratio of $L/D < 10$ is needed as the Mustang Island test piles had a slenderness ratio of $L/D = 34.4$. Briaud et al. [5] postulate that the soil response depends on the flexibility of the pile. Criteria for stiff versus flexible behaviour of piles have been proposed by various authors, e.g. Dobry et al. [6]; Budhu and Davies [7]; and Poulus and Hull [8]. A pile behaves rigidly according to the following criterion, cf. [8]:

$$L < 1.48 \left(\frac{E_p I_p}{E_s} \right)^{0.25} \tag{2}$$

in which L is the embedded length, I_p is the second moment of inertia of the pile, and E_p and E_s is Young's modulus of elasticity of the pile and the soil, respectively. Similarly, the criterion for a flexible pile behaviour is:

$$L > 4.44 \left(\frac{E_p I_p}{E_s} \right)^{0.25} \tag{3}$$

According to Equation (2) a steel monopile with an outer diameter of 4 m, an embedded length of 20 m and a wall thickness of 0.05 m behaves rigidly if $E_s < 7.6$ MPa. In contrast, the pile exhibits a flexible behaviour if $E_s > 617$ MPa. Even dense sands have $E_s < 100$ MPa, so in accordance to Equation (2) the recently installed monopiles for offshore foundations behaves more rigidly than flexible.

For modern wind turbine foundations only small pile head rotations are acceptable. Furthermore, the strict demands to the total stiffness of the system due to resonance in the serviceability mode increase the significance of the p–y curve's initial slope and hereby the initial stiffness of the soil-pile system. It seems questionable that the initial stiffness of the p–y curves are independent of the pile properties among these the pile diameter. The research within the field of diameter effects gives contradictory conclusions. Most researchers, cf. Terzaghi [9]; Ashford and Juirnarongrit [10]; and Fan and Long [11], conclude that the effect of the diameter on the initial stiffness of the p–y curves are insignificant. In contradiction to this Carter [12] and Ling [13] postulate that the initial stiffness of the p–y curves has a linear relation with the pile diameter. However, as well as the research is based on a very limited number of tests, most research considers only relatively slender piles, which is rarely the case for offshore wind turbine foundations.

In the present paper the effects of diameter on static p–y curves for piles in homogeneous sand are assessed in two ways. Firstly in terms of six small-scale tests carried out in a pressure tank at varying effective stress levels in the Laboratory of Foundation at Aalborg University, Denmark. Secondly a numerical model, calibrated to the laboratory tests, is extended to simulation of large-scale offshore wind turbine foundations. The numerical model is made by means of the commercial programme $FLAC^{3D}$. The main focus in the assessment of the p–y curves is the initial stiffness.
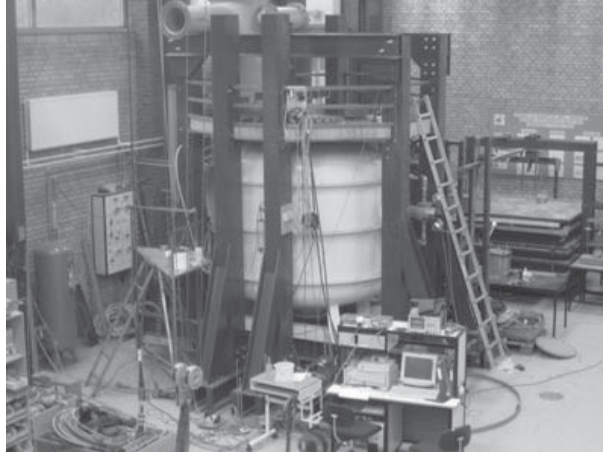
Figure 2: Pressure tank at Aalborg University, Denmark.

2 Laboratory test

2.1 Setup

When conducting small-scale tests in sand at 1-g an often introduced source of error is the low stress levels causing the angle of internal friction to vary strongly with stresses. Hence, it is an advantage to increase the effective stresses to a level where the angle of internal friction, φ_{tr}, is independent of a possible stress variation during the tests. This is possible in the pressure tank at Aalborg University, cf. Figure 2. The pressure tank is furnished with trap doors in order to enable preparation of the test setup prior to each test.

The increase in effective stress level is created by separating the lower part of the pressure tank, containing saturated soil, from the upper part by use of an elastic membrane. In this way the saturated soil is sealed from the air above. By increasing the air pressure in the upper part, a homogenous increase in stresses is introduced at the soil surface via the elastic membrane. To ensure limited excessive pore pressure, the soil is connected to an ascension pipe, leaving the soil fully saturated but with stresses applied as effective stresses only. A cross sectional view of the test setup is shown in Figure 3.

A total number of six tests have been conducted at overburden pressures, $P_0 = 0$ kPa, $P_0 = 50$ kPa and $P_0 = 100$ kPa. The overburden pressure is equal to the pressure at the elastic membrane. The conducted tests are quasi-static tests on two instrumented aluminium pipe piles with outer diameters of $D = 60$ mm and $D = 80$ mm, respectively. Both piles have a slenderness ratio of $L/D = 5$ corresponding to an embedded length of 0.3 m and 0.4 m, respectively. Both piles have a wall thickness of 5 mm and are closed-ended in order to protect the strain gauges and their corresponding cords against water. The piles are installed in one continuous motion by means of a hydraulic piston mounted vertically on the top of the pressure tank. After installation the

1. Ascension pipe
2. Displacement transducers
3. Monopile
4. Wire
5. Membrane
6. Force transducer
7. Actuator
8. Saturated sand
9. Saturated gravel
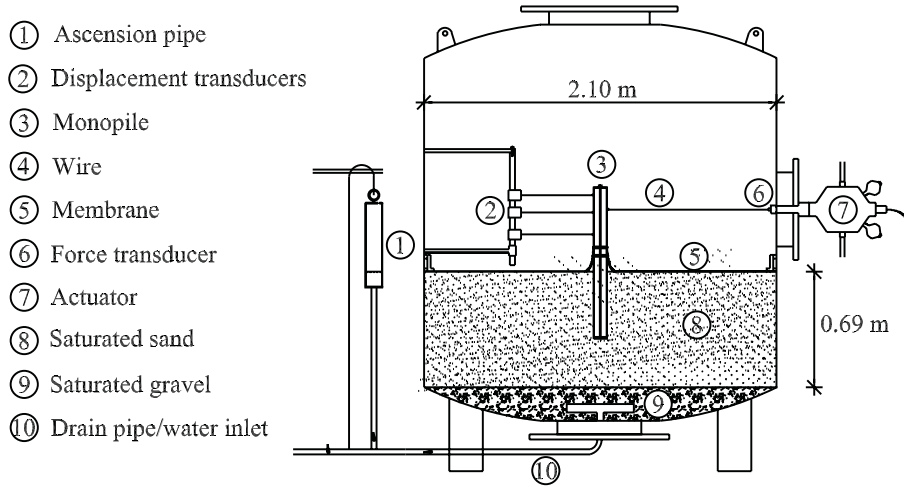10. Drain pipe/water inlet

Figure 3: Pressure tank - test setup.

sand is mechanically vibrated. In this way a homogenous compaction of the soil is ensured.

A hydraulic piston, cf. 7 in Figure 3, is employed horizontally at the pressure tank to actuate the test piles with a vertical load eccentricity of 0.37 m above the soil surface. The pile and the hydraulic piston is connected by means of a steel wire. In order to measure the force acting on the pile a force transducer is connected in series of the hydraulic piston and the wire. Lateral deflections are measured at three levels (0.2, 0.37 and 0.48 m) above the soil surface by means of wire transducers. A total number of 10 strain gauges are mounted on the pile beneath the soil surface. The strain gauges are located at five levels as shown in Figure 4. At each level two foil strain gauges are mounted in grooves milled on the outside of the pile with a mutual angle of $180°$ oriented in the plane of the horizontal load. The grooves are sealed to protect the strain gauges.

The two employed piles have been calibrated prior to the testing and have the following pile bending stiffness': $EI_{p,80} = 52.4$ kNm^2; $EI_{p,60} = 24.9$ kNm^2. The Poisson's ratio of the aluminium piles is considered to be $\nu = 0.33$.

The soil in the pressure tank consists of 0.69 m fully saturated Baskarp Sand no. 15 which is a graded sand from Sweden, with the characteristics given in Table 1.

Specific grain density d_s	2.64
Maximum void ratio $e_{\max}$	0.858
Minimum void ratio $e_{\min}$	0.549
$d_{50} = 50$ % - quantile	0.14 mm
$U = d_{60}/d_{10}$	1.78

Table 1: Material properties for Baskarp Sand No. 15, after Larsen [14].
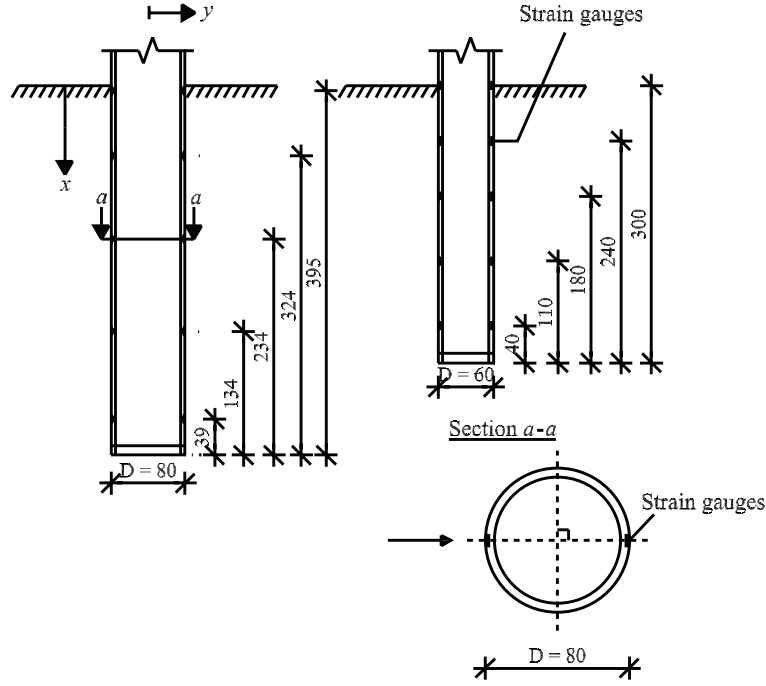
5

Figure 4: Strain gauge levels. All measurement levels are identical. Measures are in mm.

The homogeneous compaction before each test is controlled by conducting cone penetration tests (CPT). Four CPT's with a distance of 0.5 m from the center of the pile and two 0.16 m from the neutral sides of the pile, i.e. the sides perpendicular to the load direction, are conducted. The employed CPT is a prototype probe with a diameter of 15 mm. Based on the measured cone resistance, q_c, as function of depth the material properties of the sand have been derived. The derived parameters are given in Table 2 for the six tests. The parameters are derived in accordance to Ibsen et al. [15] where the angle of internal friction, ϕ_{tr}, and the tangential Young's modulus of elasticity, E_0, is related to the stress level. Due to the high angles of internal friction the sand is considered as very dense. For the tests without overburden pressure E_0 is calibrated against the numerical models as the employed formulas produce large uncertainties at low stress levels.

2.2 Analysis of the tests results

Figure 5 presents the load-displacement relationships at different overburden pressures measured at the height of the hydraulic piston. As shown in the figure the ultimate resistance is strongly dependent on the vertical stresses.

The p–y curves are traditionally derived on basis of the bending moment distribu-

6

	D	P_0	φ_{tr}	Relative density I_D	Unit weight γ'	E_0
	[mm]	[kPa]	[°]	[-]	[kN/m^3]	[MPa]
Test 1	80	0	52.6	0.79	10.2	-
Test 2	80	100	45.9	0.79	10.2	41.1
Test 3	80	50	48.5	0.79	10.2	25.4
Test 4	60	0	52.2	0.76	10.1	-
Test 5	60	50	48.3	0.78	10.1	24.9
Test 6	60	100	45.1	0.75	10.1	37.4

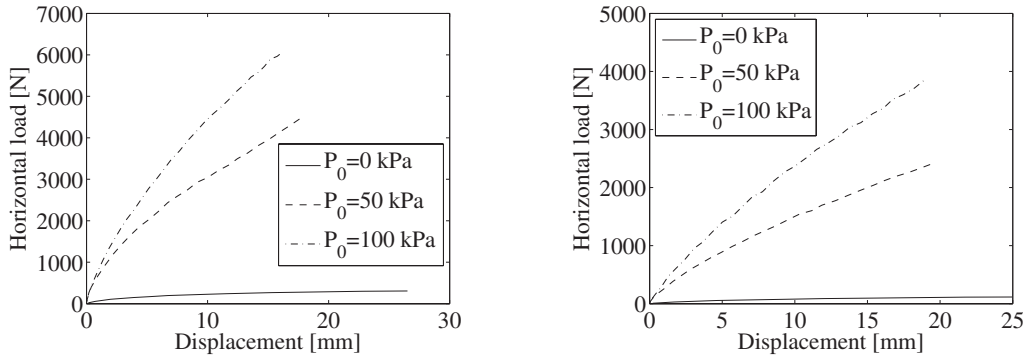Table 2: Test programme and material properties calculated for the six tests.

Figure 5: Load-displacement for different pressures at the height of the hydraulic piston. Left: $D = 0.08$ m, $L = 0.4$ m. Right: $D = 0.06$ m, $L = 0.3$ m.

tion along the pile, $M(x)$, and the pile bending stiffness, $E_p I_p$:

$$y(x) = \int \int \frac{M(x)}{E_p I_p} dx dx \qquad (4)$$

$$p(x) = \frac{d^2 M(x)}{dx^2} \qquad (5)$$

The double integration of the discrete data points with respect to depth does not implement significant errors. However, double differentiation of the discrete signal gives an amplification of measurement errors. In order to minimise these errors the piecewise polynomial curve fitting method described by Yang and Liang [16] is employed in this paper. When using this method the moment distribution is estimated by fitting five succesive moment data points to 3. order polynomials.

Figure 6 presents the lateral pile displacements with depth at the three different stress levels for the two pile diameters. A prescribed deflection of 10 mm at the level of the hydraulic piston are outlined. The lateral displacement can be separated into two components: deformation of the pile due to bending moments and rotation of the pile as a rigid object. The pile deformation due to bending moments is calculated according to Equation (4). The pile rotation is obtained by the displacement trans-
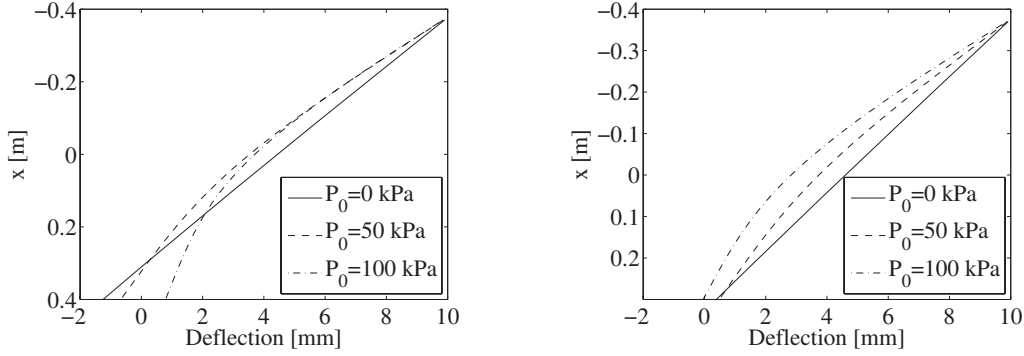
Figure 6: Lateral pile displacement at different stress levels. Left: $D = 0.08$ m, $L = 0.4$ m. Right: $D = 0.06$ m, $L = 0.3$ m.

ducers at the top of the pile and at the height of the hydraulic piston. Based on the known vertical distance between the two displacement transducers and the measured horizontal displacements the rotation of the pile at the height of the hydraulic piston is obtained. As shown the piles behave almost as rigid objects when $P_0 = 0$ kPa. When applying overburden pressure the pile deformation caused by bending is more significant, but still with a pile deflection primarily depending on the rotation. Due to the rigid behaviour of the pile, the deflection at the pile toe must be negative which is not the case for most of the tests. This could be caused by the relatively small vertical distance between the displacement transducers which could lead to large uncertainties when determining the rotation.

Figure 7 presents normalised p–y curves at two depths. The observations lead to the conclusion that the initial stiffness of the p–y curve is highly dependent on the pile diameter with the highest stiffness relating to the largest pile diameter. When $P_0 = 0$ kPa the initial stiffness of the pile with an outer diameter of 80 mm is in the range of 3–4 times higher than the stiffness for the pile with an outer diameter of 60 mm.

3   Numerical modeling of monopile under static lateral loading

A three-dimensional numerical model has been constructed in the commercial pro-gramme *FLAC*^{3D} with the objective to examine the behaviour of laterally loaded, large-diameter piles in cohesionless soil. *FLAC*^{3D} is a dynamic, explicit finite differ-ence solver based on the finite difference method. A Mohr–Coulomb material model with tension cut-off has been employed.
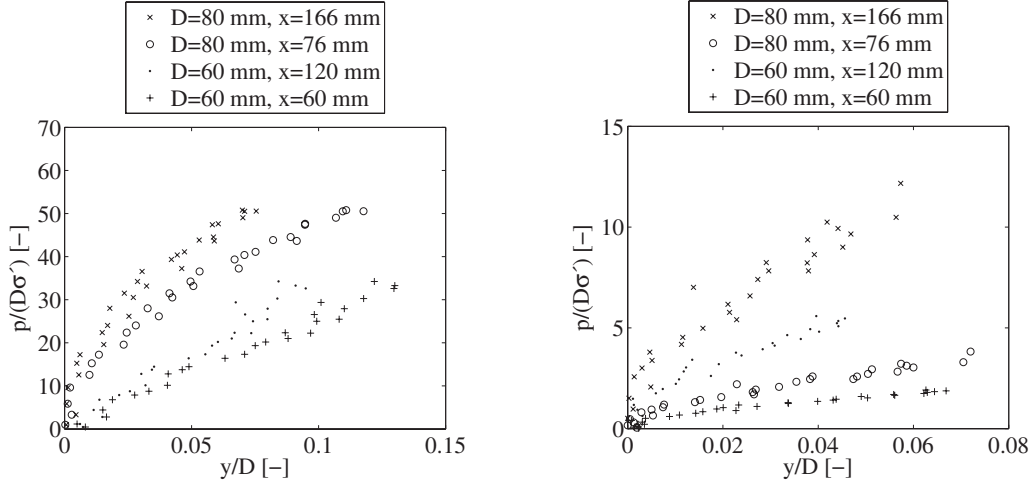
8

Figure 7: Relationship between normalised soil resistance and normalised displacement for the two pile diameters. Left: $P_0 = 0$ kPa. Right: $P_0 = 100$ kPa.

3.1 Construction of numerical model in $FLAC^{3D}$

Due to symmetric loading conditions only one half of the pile and surrounding soil are modelled. The pile is modelled as a solid cylinder, in contrast to the closed-ended pipe piles employed in the laboratory tests. The bending stiffness of the solid piles, EI_{flac}, is equivalentet to the stiffness of the hollow test piles, $E_p I_p$, by reducing Young's modulus of elasticity. The weight of the hollow and the solid piles are in the same way equivalentet. Both the laboratory test piles and the large-scale pipe piles are equivalentet. The Poisson's ratio of the pile material is not scaled, which leads to an incorrect scaling of the shear modulus, G, and bulk modulus, K. The effect of this error is small as the pile primarily is subjected to bending.

The geometry of the model and the orientation of the coordinate system are shown in Figure 8. The grid is generated from zone elements. Each zone consist of five first order, constant rate of strain, tetrahedral subelements. The outer boundaries of the grid when calibrating are set to the inner diameter of the pressure tank. When simulating large-scale piles the outer boundaries, are set individually for each pile. The outer diameter of the soil mass is set to $40D$ based on the recommendations by Abbas et al. [17]. The height of the grid is set to $L + 15$ m. It has been observed that the zone of failure does not reach the outer boundaries.

The soil-pile interface is modelled by means of the standard $FLAC^{3D}$ interface. A linear Coulomb shear-strength criterion is employed for the interfaces to limit the shear forces acting on the interface nodes. The interface elements allows gapping and slipping between the soil and the pile.

The horizontal load is applied as a velocity at the nodes corresponding to $x = 0$ at the pile head. Hereby, no artificial bending moment is introduced at the pile head.
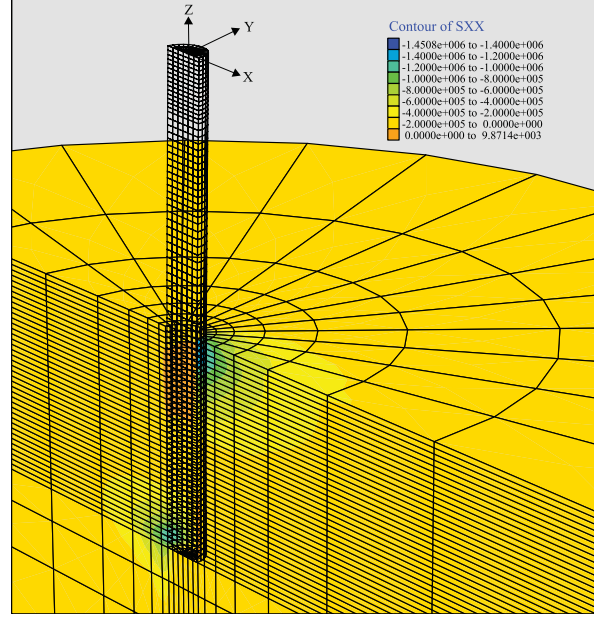
9

Figure 8: Three-dimensional mesh. The contour illustrates the horizontal stresses, s_{xx}, at a horizontal load of 5300 N, $D = 0.08$ m, $L = 0.4$ m, and $P_0 = 100$ kPa.

The calculations are executed in steps. Firstly, the initial stresses are generated for the whole model containing only soil properties. The horizontal stresses are determined by a K_0-procedure. Secondly, the pile parameters are introduced. In order to take the overburden pressure into account for the test piles an initial load is applied in these cases. When applying the overburden pressure, the pile is at first assumed smooth. When equilibrium is reached for the smooth pile the correct interface properties are employed and a new equilibrium state is computed. After reaching equilibrium in the model, velocities are applied to the pile head in small increments in order to minimise inertial forces in the system. Further, damping is employed in the system.

3.2 Calibration of numerical model

On the basis of the derived soil parameters given in Table 2 the interface properties of the numerical model in $FLAC^{3D}$ have been calibrated. The soil parameters are assumed to remain constant with depth. An example of the calibration is shown in Figure 9 where the measured lateral displacement at three levels, symbolised by a, above the soil surface is compared with the results obtained from the numerical model. Figure 10 presents the calibrated and measured bending moment distribution at a horizontal load of 2100 N. The bending moment distribution along the pile is computed by means of Naviers formula correlating stresses and moments. The bending moment is calculated from two points ($y = 0$, $x = \pm D/2$) at each level of the pile. Hereby, the average vertical stress corresponding to the axial force is eliminated. As shown in Figure 9 and 10, the agreement between the experimental and computed values is
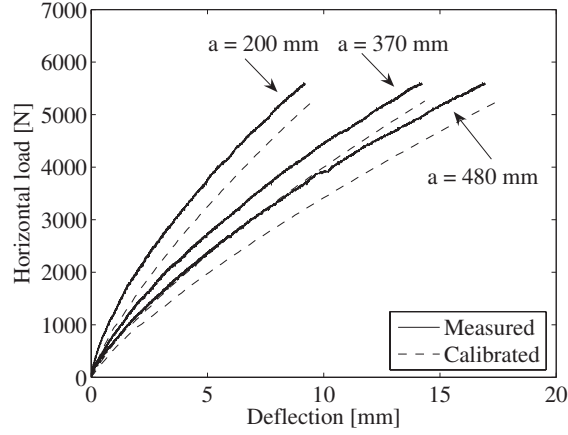
Figure 9: Load-displacement relationship at three levels above soil surface, for $D = 0.08$ m, $L = 0.4$ m, and $P_0 = 100$ kPa.

good, as the parameters listed in Table 2 have been employed in *FLAC*^{3D}. Similar analyses have been conducted for the remaining five tests with similar results. Based on these calibrations the wall friction angle, δ, is set to 30°.

3.3 Simulation of large-scale monopiles

Three steel pipe piles with pile diameters of 3 m, 5 m, and 7 m, respectively are simulated with the objective to examine the behaviour of large-diameter non-slender monopiles. The embedded length is 20 m, the wall thickness is 0.05 m and the vertical load eccentricity is 15 m.

The material parameters for the soil and pile employed in the large-scale analyses are listed in Table 3.

Effective unit weight of the soil γ'	10 kN/m^3
Angle of internal friction φ_{tr}	40°
Dilatancy angle ψ_{tr}	10°
Cohesion c	0.1 kN/m^2
Relative density I_D	80%
Poisson's ratio for the soil ν_s	0.23
Coefficient of horizontal earth pressure at rest K_0	1-sin(φ_{tr})
Young's modulus of elasticity for the pile E_p	210 GPa
Poisson's ratio for the pile ν_p	0.3
Unit weight of the pile γ_p	78.5 kN/m^3

Table 3: Material properties employed in the large-scale analyses.

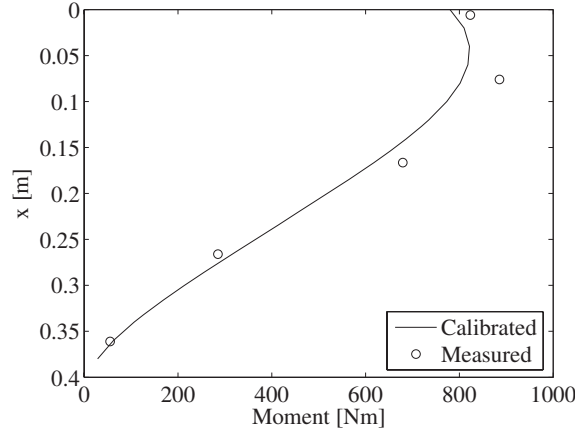The tangential Young's modulus of elasticity for the soil, E_0, is varied with the mi-

Figure 10: Distribution of bending moment with depth at a horizontal load of 2100 N, $D = 0.08$ m, $L = 0.4$ m, and $P_0 = 100$ kPa.

nor principal stress σ_3' on basis of Equation (6) proposed by Ibsen et al. [15]. Equation (6) is valid for Baskarp Sand no. 15. The factor of 1.82 specifies, according to *Plaxis 2D* [18], the relation between E_0 and E_{50}.

$$E_0 = 1.82(0.6322 I_D^{2.507} + 10920) \left(\frac{c \cdot cos(\varphi_{tr}) + \sigma_3' \cdot sin(\varphi_{tr})}{c \cdot cos(\varphi_{tr}) + \sigma_3'^{ref} \cdot sin(\varphi_{tr})} \right)^{0.58} \text{[kN/m}^2\text{]} \quad (6)$$

In the empiric formula I_D should be implemented in percent and $\sigma_3'^{ref} = 100$ kPa.

Figure 11 presents the lateral pile deflection with respect to depth. The applied displacements, corresponding lateral load, and depth of maximum moments are outlined in Table 4 for the three simulated piles. The deflection of the piles shows a rigid body motion which is most significant for $D = 7$ m. The more rigid pile behaviour for increasing diameters is in good accordance with Poulus and Hull [8] as the employed pile bending stiffness increases for increasing pile diameter. Due to the rigid pile behaviour, a significant negative deflection at the pile toe is observed. The point of zero deflection is located at a depth of approximately $x = 15$ m for all three piles.

Outer diameter [m]	Displacement [m]	Load [MN]	Depth of max. moment [m]
3	0.58	6.4	4.8
5	0.24	8.8	5.0
7	0.84	21.4	4.9

Table 4: Applied displacements, equivalent loads, and depth of maximum moments for the three pile diameters.

Figure 12 presents the distribution of bending moment along the piles. It is observed that the maximum bending moment is located at a depth of approximately 5
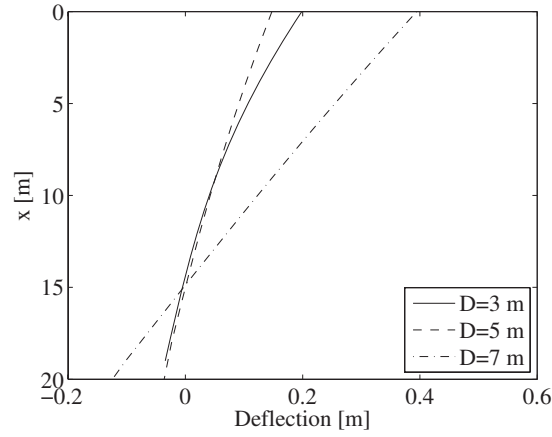
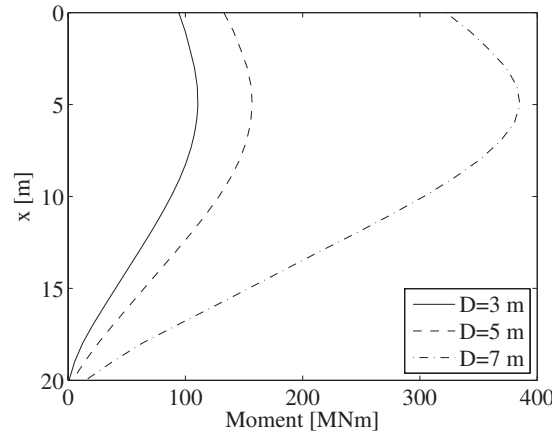Figure 11: Lateral pile deflection for the three large-scale piles.

Figure 12: Bending moment distribution along the piles.

m for all the piles, cf. Table 4. As the point of zero deflection for the three piles are situated approximately at the same depth, the depth of maximum moment are as well. For the piles with $D = 5 - 7$ m the bending moment is non-zero at the pile toe. This may be due to a combination of large diameter, large rotations and the solid base.

Figure 13 shows the p–y curves obtained at a depth of $x = 2$ m. Further, the p–y curves according to API [3], cf. Equation (1), are outlined in the figures. As expected the ultimate soil resistance increases for increasing pile diameter. Further, the initial part of the curves, is stiffer for the API p–y curves compared to the p–y curves obtained by means of $FLAC^{3D}$. The ultimate soil resistance of the API p–y curves has some degree of conservatism in the case of very large diameters. This is however, not observed for the pile with $D = 3$ m. Furthermore, the p–y curves obtained from the three-dimensional numerical model do not reach a steady state at
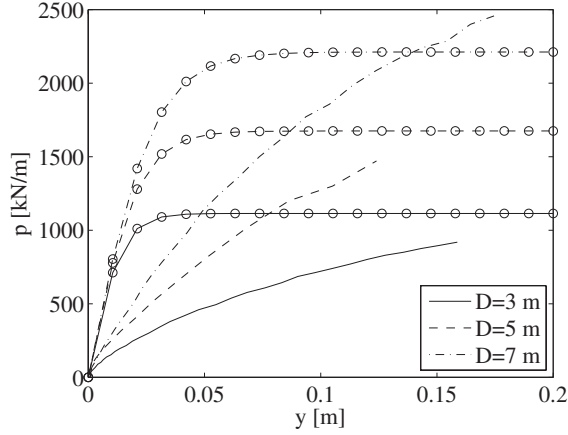
13

Figure 13: Comparison of API p–y curves marked with (o) and the p–y curves obtained by the numerical model for the three piles, respectively.

the applied displacements.

The variation of initial stiffness with depth, $E_{py}^* = \frac{\delta p}{\delta y}$, $y = 0$, is presented in Figure 14 for the three pile diameters. The initial stiffness is observed to increase for increasing pile diameters. The design regulations, e.g. DNV [2] and API [3], suggest that the initial modulus of subgrade reaction, k, and hereby also the initial stiffness E_{py}^*:

$$E_{py}^* = kx \tag{7}$$

is independent of the pile diameter, which is in contrast to the variation of initial stiffness shown in Figure 14. The p–y curves obtained near the point of zero deflection is characterised by a lot of scatter causing large uncertainties for the initial stiffness at large depths.

The magnitudes of k in Equation (7) are outlined in Table 5 at $x = 2 - 7$ m where this assumption is reasonable. As indicated in Table 5, k is highly dependent on the pile diameter; increasing diameter results in an increase in k. This observation is most significant when comparing the results for the piles with $D = 3$ m and $D = 5$ m. For dense sand ($\varphi_{tr} = 40°$) the offshore design regulations recommend $k = 40000$ kN/m^3. This cannot be validated based on the analyses since k ranges between 9700–29000 kN/m^3. In order to validate the results in Table 5 more research is needed.

According to Figure 14 there is no linear variation of $E_{py}^* = kx$ with depth. Lesny and Wiemann [19] propose a power function for the variation of E_{py}^* with depth:

$$E_{py}^* = E_{py,ref}^* \left(\frac{x}{x_{ref}} \right)^a \tag{8}$$

where $E_{py,ref}^*$ denotes the initial stiffness at a reference depth, x_{ref}, and a is a factor depending on the relative density of the sand. According to [19] the factor a is to be set to 0.6 for medium dense sands.
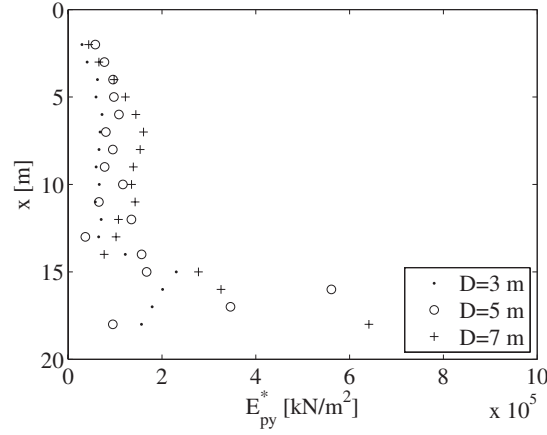
14

Figure 14: Initial stiffness versus depth.

	D=3 m	D=5 m	D=7 m
x=2 m	14799	28964	21891
x=3 m	13550	25798	21846
x=4 m	15663	23921	24547
x=5 m	11881	19532	24440
x=6 m	12045	18065	24077
x=7 m	9747	11475	22963

Table 5: Initial modulus of subgrade reaction, k. k are specified in [kN/m^3].

Figure 15 presents the obtained initial stiffness' from the simulations and the variations based on Equation (7) and (8) for $D = 3$ m. The two expressions, cf. Equations (7) and (8), are identical when $a = 1$. As a reference initial stiffness, $E^*_{py,ref}$, the initial stiffness at $x_{ref} = 2$ m is employed. Figure 15 indicates that the linear expression employed in the design regulations fits the obtained E^*_{py} well until a depth of approximately 5 m. Beneath this depth the linear expression highly overestimates E^*_{py}, implying that the soil response is non-conservative at large depths. The power function fits the obtained E^*_{py} well until a depth of 13 m. The obtained by means of $FLAC^{3D}$ E^*_{py} beneath $x = 13$ m are influenced by the point of zero deflection. For the remaining pile diameters a similar variation of E^*_{py} with depth is found, giving that the expression in the offshore design regulations overestimates the soil-pile interaction for large-diameter monopiles en sand at large depth.

3.4   Comparison of the results with a Winkler model approach

A traditional Winkler model has been constructed in order to compare the results obtained from the three-dimensional numerical model with the recommendations in
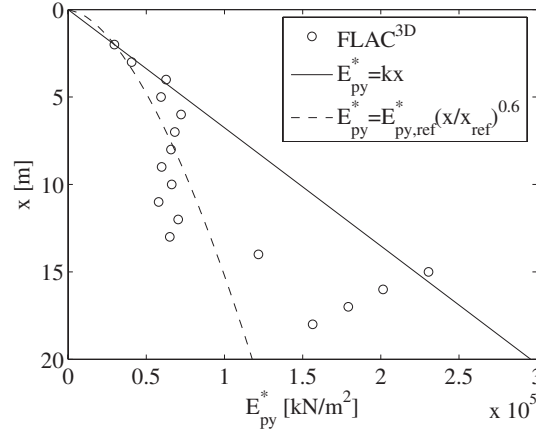
15

Figure 15: Variation of E_{py}^* as function of depth, $D = 3$ m, $x_{ref} = 2$ m, and $E_{py,ref}^*$=29598 kN/m^2.

the design regulations. The nonlinear soil behaviour is modelled using the API [3] p–y curves, cf. Equation (1). The comparison between the three-dimensional numerical model and the Winkler model approach is performed, with the same pile geometry, and soil conditions as listed in Table 3. Figure 16 presents the load-displacement relationships at the pile top located 15 m above seabed ($D = 3$ m) obtained from $FLAC^{3D}$, and the Winkler model approach. The power function, cf. Equation (8), and the recommendations in API [3], with $k = 40000$ kN/m^3 and $k = k_{ref}$ at $x = 2$ m, respectively have in turn been implemented in the Winkler model approach. Figure 16 indicates that the expression employed in API [3] highly overestimates the strength of the soil at all deflections compared to $FLAC^{3D}$. In accordance with Table 5 this is expected as the initial modulus of subgrade reaction, k, is overestimated compared to the values calculated by means of FLAC^{3D}. The linear expression, cf. Equation (7), with k_{ref} as the value obtained at $x_{ref} = 2$ m gives reasonable results until a deflection of approximately 0.1 m. At higher deflections there is a considerable difference between the deflections determined by $FLAC^{3D}$ and the linear expression. When employing the power function, cf. Equation (8), in the Winkler model approach the initial part of the load-displacement relationship fits very well until a deflection of 0.2 m. At higher deflections an overestimation of the horizontal load is observed compared to $FLAC^{3D}$. However, the difference is less than obtained by employing the linear expression in the Winkler model. Similar load-displacement behaviour has been observed for the piles with $D = 5$ m and $D = 7$ m.

For modern wind turbine foundations only small deformations/rotations are allowed. Therefore, it is desirable that the initial part of the curves fits the pile behaviour well, which is the case for the power function employed in the Winkler model approach. Hence, it can be concluded that the Winkler model approach is useful when a proper variation of the initial stiffness associated with the p–y curves is employed.
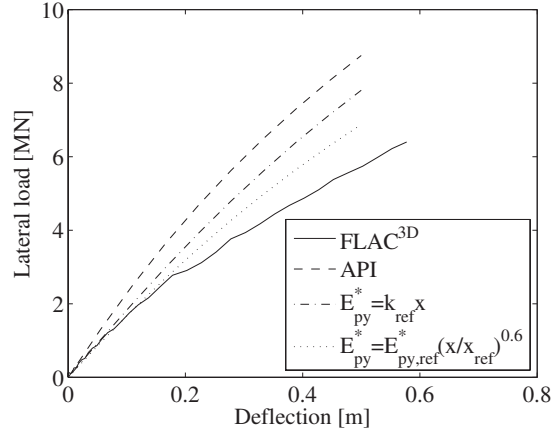
16

Figure 16: Load-displacement relationships at the pile top calculated by *FLAC*^{3D} compared with the Winkler model approach incorporating API ($k = 40000$ kN/m^3), API (k_{ref}), and the power function, cf. [19], respectively.

4 Conclusion

This paper presents the results of six quasi-static tests on two non-slender laterally loaded monopiles in a pressure tank. The tests are reproduced by means of a three-dimensional numerical model constructed in *FLAC*^{3D} and extended to large-scale monopiles with pile diameters varying between $D = 3 - 7$ m. This corresponds to slenderness ratios between $L/D = 2.9 - 6.7$. The conclusions that can be drawn are:

- The non-slender piles deflects as almost rigid objects given only one point of zero deflection. Hereby, negative deflections at the pile toe are observed.

- The initial modulus of subgrade reaction, k, is highly affected by the pile diameter; increasing diameter results in an increase in k. This is observed in connection with both the tests and the numerical analyses. This contradicts the recommendations in the offshore design regulations. k is varying between 9700-29000 kN/m^3 at small depths when increasing the diameter from 3–7 m.

- The design regulations recommends a linear variation of initial stiffness with depth. This recommendation is non-conservative at large depths. Here, the soil response is overestimated. A non-linear variation of initial stiffness with depth proposed by Lesny and Wiemann [19] provides a good agreement when compared to the results from the three-dimensional numerical model.

- More research is needed in order to update the p–y curves recommended in the offshore design regulations to large diameter non-slender monopiles.

17

Acknowledgements

References

[1] J. Ubilla, T. Abdoun, T. Zimmie, "Application of in-flight robot in centrifuge modeling of laterally loaded stiff pile foundations", Physical Modelling in Geotechnics, Taylor & Francis Group, London, ISBN 0-41-41586-1,259-264, 2006.

[2] DNV, "Foundations - Classification Notes No 30.4", Det Norske Veritas, Det Norske Veritas Classification A/S, 1992.

[3] API, "Recommended practice for planning, designing, and constructing fixed offshore platforms - Working stress design", API RP2A-WSD, American Petrolium Institute, Washington D.C., 21. edition, 1993.

[4] W.R. Cox, L.C. Reese, B.R. Grubbs, "Field Testing of Laterally Loaded Piles in Sand", Proceedings of the Sixth Annual Offshore Technology Conference, Houston, Texas, 2079, 1974.

[5] J.L. Briaud, T.D. Smith, B.J. Meyer, "Using pressuremeter curve to design laterally loaded piles", Proceedings of the 15th Annual Offshore Technology Conference, Houston, Texas, 495-502, 4501, 1984.

[6] R. Dobry, E. Vincente, M. O'Rourke, J. Roesset, "Stiffness and Damping of Single Piles", Journal of geotechnical engineering, 108, 3, 439-458, 1982.

[7] M. Budhu, T. Davies, "Nonlinear Analysis of Laterally loaded piles in cohesionless Soils", Canadian geotechnical journal, 24(2), 289-296, 1987.

[8] H. Poulus, T. Hull, "The Role of Analytical Geomechanics in Foundation Engineering", Foundation Engineering: Current principles and Practices, 2, 1578-1606, 1989.

[9] K. Terzaghi, "Evaluation of coefficients of subgrade reaction", Geotechnique, 5(4), 297-326, 1956.

[10] S.A. Ashford, T. Juirnarongrit, "Evaluation of Pile Diameter Effect on Initial Modulus of Subgrade Reaction", Journal of Geotechnical and Geoenvironmental Engineering, 129(3), 234-242, 2003.

[11] C.C. Fan, J.H. Long, "Assessment of existing methods for predicting soil response of laterally loaded piles in sand", Computers and Geotechnics, 32, 274-289, 2005.

[12] D.P. Carter, "A Non-Linear Soil Model for Predicting Lateral Pile Response", Rep. No. 359, Civil Engineering Dept,. Univ. of Auckland, New Zealand, 1984.

[13] L.F. Ling, "Back Analysis of Lateral Load Test on Piles", Rep. No. 460, Civil Engineering Dept., Univ. of Auckland, New Zealand, 1988.

[14] K. A. Larsen, "Static Behaviour of Bucket Foundations", Department of Civil Engineering, Aalborg University, Denmark, 2008.

[15] L. B. Ibsen, M. Hanson, T. H. Hjort, M. Thaarup, "MC–Parameter Calibration for Baskarp Sand No. 15", DCE Technical Report No. 62, Department of Civil Engineering, Aalborg University, Denmark, 2009.

[16] K. Yang, R. Liang, "Methods for Deriving p–y Curves from Instrumented Lateral Load Tests", Geotechnical Testing Journal, 30(1), Paper ID GTJ100317, 2006.

[17] J. M. Abbas , Z. H. Chik, M. R. Taha, "Single Pile Simulation and Analysis Subjected to Lateral Load", Electronic Journal of Geotechnical Engineering, 13E, 1-15, 2008.

[18] Plaxis 2D, "Material Models Manual Version 9.0".

[19] K. Lesny, J. Wiemann, "Finite-Element-Modelling of Large Diameter Monopiles for Offshore Wind Energy Converters", Geo Congress 2006, February 26 to March 1, Atlanta, GA, USA, 2006.